Macromolecules
ARTICLE

Macromolecules **2010**, *43*, 4599–4608 **4599**
DOI: 10.1021/ma902353r

Novel Electroactive Proton-Doped Conducting Poly(aromatic ethers) with Good Fluorescence Properties via Electropolymerization

Baoyang Lu,[†] Jun Yan,[‡] Jingkun Xu,*[,†] Shuyun Zhou,*[,‡] and Xiujie Hu[‡]

[†]*Jiangxi Key Laboratory of Organic Chemistry, Jiangxi Science and Technology Normal University, Nanchang 330013, China, and* [‡]*Key Laboratory of Photochemical Conversion and Optoelectronic Materials, Technical Institute of Physics and Chemistry, Chinese Academy of Sciences, Beijing 100190, China*

Received October 22, 2009; Revised Manuscript Received April 10, 2010

ABSTRACT: Low-potential electrochemical polymerization of a series of aromatic ethers in boron trifluoride diethyl etherate (BFEE), such as diphenyl ether (DPE), 1,4-diphenoxybenzene (DPOB), and 2,2′-dinaphthyl ether (DNE), led to successful deposition of a new class of electrically conducting proton-doped poly(aromatic ethers) thin films exhibiting good electroactivity and high thermal stability, whereas their sulfur analogues, diphenyl sulfide (DPS) and diphenyl sulfone (DPSO), were not eletropolymerizable. FT-IR, ^{1}H NMR spectra, and computational results demonstrated that poly(1,4-diphenoxybenzene) (PDPOB) were synthesized mainly through the coupling of DPOB at *para*-positions, while the polymerization of DNE occurred probably at α- and C_6-positions of the naphthyl rings to form poly(2,2′-dinaphthyl ether) (PDNE) with complex structure. It was found that the electrodeposited poly(aromatic ethers) probably showed proton-doping nature similar to polyaniline based on FT-IR spectral results and conductivity investigation. As-formed PDPOB and PDNE were typical blue light emitters and highly fluorescent, with solution quantum yields of as high as 0.40 and 0.18, respectively. Surface morphology determination revealed that regular and homogeneous microspheres with diameters in the range from 200 nm to 1 μm were assembled on ITO electrode after electrochemical growth. Electro-oxidation of aromatic ethers therefore offers a ready route to novel conducting, redox-active, luminescent conjugated polymers. These materials open up a new, unexplored, and potentially vast area of research on poly(aromatic ethers) and hold promise for the design of a new generation of optoelectronic materials.

1. Introduction

Tremendous advancement has been made in developing various polymeric materials. As a new rising field among them, in spite of their short history, conducting polymers have been of particular significance in specialized industrial applications,[1,2] including organic electronic devices, sensors, supercapacitors, and electroluminescent materials.[3] However, even to date, despite the large amount of work devoted to the fundamental research of conducting polymers, it is widely perceived that the design and synthesis of novel conducting polymers with unique properties suffice for applications, such as good fluorescence properties, stable electroactivity, and favorable thermal stability, are still very necessary and significant and apparently also a considerable challenge.

Electrochemical polymerization, as one of fast and reliable conventional synthetic methods, has been widely employed for the generation of conducting polymers onto a conducting surface.[4] In recent years, conducting polymers synthesized from the electropolymerization of fused-ring aromatic compounds have drawn considerable attention owing to their unique properties, such as excellent fluorescence and high thermal stability, and a wide range of promising electrochemical, electronic, and optical applications.[5−17] Nevertheless, with the vast repertoire of new techniques and thoughts at our disposal, many exciting discoveries of novel structures with new and perhaps unpredictable properties are quite expected to continue in this dynamic field.

*Corresponding authors: Tel 86-791-8537029; Fax 86-791-3823357; e-mail xujingkun@tsinghua.org.cn (J.X.), zhou_shuyun@mail.ipc.ac.cn (S.Z.).

Despite significant efforts, the types of conducting polymers were focused on polythiophenes, polypyrroles, polyanilines, polyphenylenes, and a few others. Given the similarity between polyanilines, polyphenylenes, and poly(aromatic ethers), it is surprising that much less attention is paid to the electrochemical polymerization of aromatic ethers, and thus very little is known about conducting poly(aromatic ethers). Aromatic ethers such as diphenyl ether and dinaphthyl ether and their derivatives are less aromatic with decreased electron delocalization compared with fused-ring compounds,[10−17] making their electrochemical polymerization impossible in conventional electrolytes. Therefore, it is a great challenge to get high-quality poly(aromatic ethers) films by direct anodic oxidation of their monomers. On the other hand, because of their unique structures similar to aniline and benzene, aromatic ether compounds with extended π-electron systems are very promising blocks for building conducting polymers with unpredictable properties. Poly(aromatic ethers) hereby deserve much attention. Hence, the electrodeposition of high-quality poly(aromatic ethers) films is quite essential.

Herein, we report the electropolymerization performances of a series of aromatic ethers derived from diphenyl ether (as listed in Scheme 1) based on our previous work.[18] It was found that conducting poly(aromatic ethers) thin films were successfully deposited by direct anodic oxidation. Properties of the resulting polymer films, such as electrochemical behavior, structural information, polymerization mechanism, solubility, spectroscopic properties, thermal stability, electrical conductivity, and morphologies, were investigated in detail.

Published on Web 04/23/2010

Scheme 1. Chemical Structures of DPE, DNE (A), DPOB (B), DPS (C), and DPSO (D)

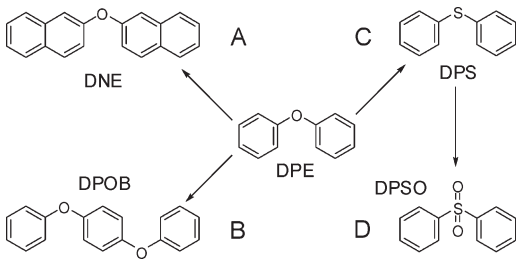

2. Experimental Section

2.1. Materials. 2,2′-Dinaphthyl ether (DNE, 98+%; Alfa Aesar), 1,4-diphenoxybenzene (DPOB, 98%; Acros Organics), diphenyl sulfide (DPS, 98+%; TCI Organic Chemicals), diphenyl sulfone (DPSO, 99+%; Alfa Aesar), commercial high-performance liquid chromatography grade acetonitrile (Guangfu Fine Chemical Research Institute, Tianjin, China), 25% ammonia (Ji'nan Chemical Reagent Co., Shandong, China), and concentrated sulfuric acid (SA, 98%; Ji'nan Chemical Reagent Co., Shandong, China) were used as received. BFEE ($(1.12-1.14) \times 10^3$ g L^{-1}, BF_3 = 48.24%; Changyang Chemical Plant, Beijing, China) was purified by distillation and stored at 0 °C before use. Dimethyl sulfoxide (DMSO, analytical grade; Tianjin Bodi Chemicals Co. Ltd., China) used directly without further purification. Tetrabutylammonium tetrafluoroborate (TBATFB, 98%; Acros Organics) was dried under vacuum at 60 °C for 24 h before use. Other reagents were all A.R. grade and used as received without further treatment.

2.2. Electrosynthesis and Electrochemical Tests. The electrochemical tests and polymerization of the monomers were performed in a one-compartment cell using a potentiostat−galvanostat (model 263A, EG&G Princeton Applied Research) under computer control. For electrochemical tests, the working and counter electrodes were Pt wire with a diameter of 0.5 mm and stainless steel wire with a diameter of 1 mm, respectively. They were placed 5 mm apart during the tests. To obtain a sufficient amount of the polymer films for characterization, ITO or Pt and stainless-steel sheets with surface areas of 4 and 6 cm^2 each were used as the working and counter electrodes, respectively. These electrodes were carefully polished with abrasive paper (1500 mesh), cleaned successively with water and acetone, and then dried in air before each experiment. An Ag/AgCl electrode directly immersed in the solution served as the reference electrode, and it revealed sufficient stability during the experiments. All the solutions were deaerated by a dry nitrogen stream and maintained under a slight overpressure through all the experiments. The polymer films were grown potentiostatically, and their thickness was controlled by the total charge passed through the cell, which was read directly from the current−time ($I-t$) curves by computer. After polymerization, the polymer films were washed repeatedly with anhydrous diethyl ether to remove the electrolyte and monomers. For spectral analyses, the polymer films were dedoped with 25% ammonia for 3 days and then washed repeatedly with pure water. Finally, the polymer film was dried at 60 °C under vacuum for 24 h.

2.3. Characterization. The electrical conductivity of the obtained polymer films was determined by applying a conventional four-probe technique with free-standing films or pressed pellets of the samples by the use of 220 programmable current source and a Keithley 2700 multimeter under computer control (Labview 7.0). The details and sketch map of the arrangement of four probes are shown in Scheme S1. Measurements of PDPOB was made on direct-electrodeposited free-standing films (length: 1.5 cm; width: 0.5 cm; thickness: about 10 μm) while that of PDNE was performed by pressing the obtained polymer powder under a pressure of 15 MPa into sample pellets (length: 1.5 cm; width: 0.5 cm; thickness: 0.2 cm). The electrical conductivity (σ) of the samples is calculated according to the equation given as follows:

$$\sigma = \frac{1}{V}\frac{L}{T\phi} \tag{1}$$

Fluorescence spectra were determined with an F-4500 fluorescence spectrophotometer (Hitachi). The fluorescence quantum yields ($\phi_{overall}$) of the soluble samples were measured by using anthracene in acetonitrile (standard, ϕ_{ref} = 0.27) as a reference and calculated based on the expression[19]

$$\phi_{overall} = \frac{n^2 A_{ref} I}{n_{ref}{}^2 A I_{ref}}\phi_{ref} \tag{2}$$

where n, A, and I denote the refractive index of the solvent, the absorbance at the excitation wavelength, and the intensity of the emission spectrum, respectively.

Infrared spectra were recorded using a Bruker Vertex 70 Fourier transform infrared (FT-IR) spectrometer with samples in KBr pellets. Ultraviolet−visible (UV−vis) spectra were measured with a Perkin-Elmer Lambda 900 UV−vis−near-infrared (NIR) spectrophotometer. The ^{1}H NMR spectra were recorded on a Bruker AV 400 NMR spectrometer with d_6-DMSO as the solvent and tetramethylsilane as an internal standard (TMS, singlet, chemical shift: 0.0 ppm). Gel permeation chromatography (GPC) measurements of the soluble part of the polymers were performed in tetrahydrofuran with a Waters Breeze GPC system. MALDI-TOF (matrix-assisted laser desorption ionization/time-of-flight) MS spectra were carried out on a Bruker MICROFLEX mass spectrometer. Thermogravimetric analysis (TGA) was performed with a Pyris Diamond TG/DTA thermal analyzer (Perkin-Elmer) under a nitrogen stream from 300 to 1020 K at a heating rate of 10 K min^{-1}. Scanning electron microscopy (SEM) measurements were made with a cold field emission scanning electron microscope S-3000N (Hitachi).

2.4. Details of Computations. All calculations were carried out using the Gaussian 03 program.[20] DPOB and DNE were optimized without symmetry constraints using a hybrid density functional[21,22] and Becke's three-parameter exchange functional combined with the LYP correlation functional (B3LYP)[23,24] and with the 6-31G(d,p) basis set (B3LYP/6-31G(d,p)). Vibrational frequencies were evaluated at the same level to identify the real minimal energy structures.

3. Results and Discussion

3.1. Cyclic Voltammetry. The electrochemical performances of the monomers (DNE, DPOB, DPS, and DPSO) were first examined by cyclic voltammetry in acetonitrile containing 0.1 mol L^{-1} TBATFB as the supporting electrolyte, as shown in Figure S1. It can be seen that cyclic voltammograms (CVs) of these monomers in acetonitrile solution showed no apparent redox waves, and after successive potential scans, no polymer film was formed on the electrodes at all, implying that electropolymerization of these monomers are not feasible in acetonitrile. Additionally, the margins among the onset oxidation potentials of DNE, DPOB, and DPS (from the first cycle of CVs in Figure S1) were narrow (approximately 1.41, 1.42, and 1.47 V, respectively), lower than that of DPE (1.62 V). This phenomenon can be attributed to the similar structures of these compounds. However, DPSO was much more difficult to be oxidized (2.25 V), mainly caused by the strong electron-withdrawing sulfonyl group in the molecule.

On the other hand, cyclic voltammetry of the four monomers were also investigated in BFEE, an excellent

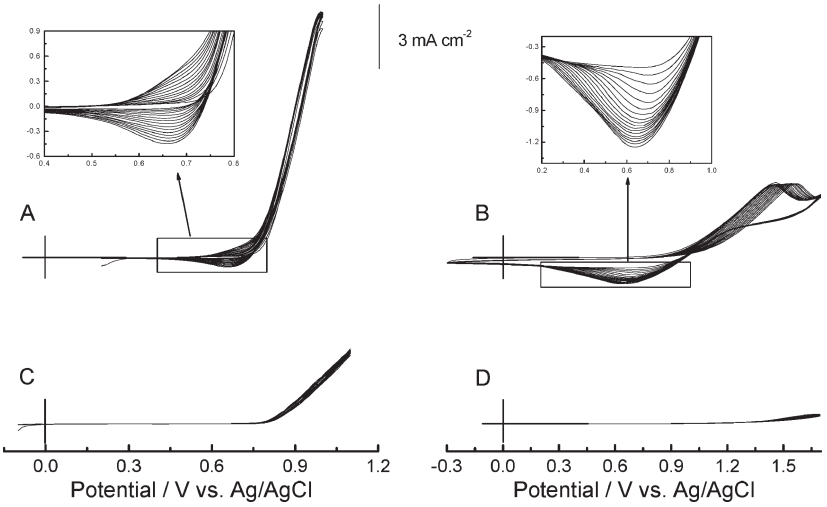

Figure 1. CVs of DNE (A), DPOB (B), DPS (C), and DPSO (D) in BFEE. Monomer concentration: 0.02 mol L^{-1}. Potential scan rate: 100 mV s^{-1}.

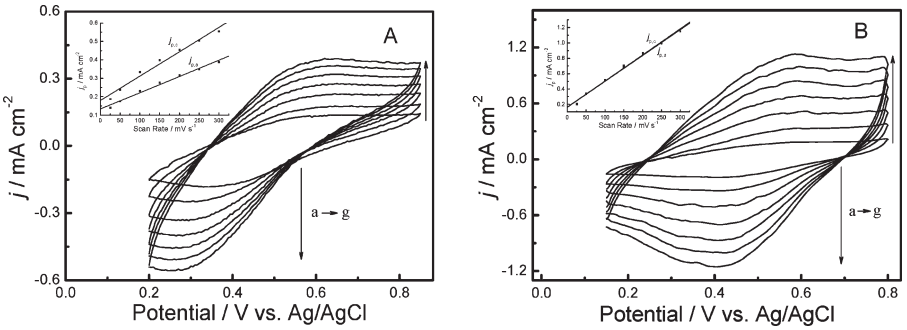

Figure 2. CVs of PDNE films prepared from BFEE containing 10% SA in monomer free BFEE containing 10% SA (A) and in concentrated SA (B) at potential scan rates of (a) 25, (b) 50, (c) 100, (d) 150, (e) 200, (f) 250, and (g) 300 mV s^{-1}. Inset: plots of redox peak current densities vs potential scan rates. j_p is the peak current density, and $j_{p,a}$ and $j_{p,c}$ denote the anodic and cathodic peak current densities, respectively.

electrolyte[25−27] in which many fused-ring compounds have been successfully electropolymerized.[10−18] The onset oxidation potentials of DNE, DPOB, DPS, and DPSO were 0.76, 0.80, 0.83, and 1.42 V, respectively (from the first cycle of CVs in Figure 1), which are greatly lowered compared with those in acetonitrile. The reason lies in the fact that BFEE can interact with the aromatic ring of these compounds, which reduced the resonance stability of the corresponding monomers through the formation of π-complexes between the monomers and BFEE, thus making electron loss from the monomers much easier.[28] Successive potential scans of DNE and DPOB (Figure 1A,B) led to the formation of the corresponding films. The increase of anodic and cathodic peak current densities in CVs implied that the amount of the polymer film increased on the electrode surface. The broad redox waves of the polymer films may be ascribed to the wide distribution of the polymer chain length or the conversion of conductive species on the polymer main chain from the neutral state to polarons, from polarons to bipolarons, and finally from bipolarons to the metallic state. The potential shift of the current wave maximum provided information about the increase of the electrical resistance of the polymer film and the overpotential needed to overcome this resistance. For DPS and DPSO, however, they could not electrochemically polymerize in BFEE even though the onset oxidation potentials were greatly lowered (Figure 1C,D). This phenomenon may be attributable to the following reasons: (1) the sulfur atom in DPS changes the electronic structure of the molecule substantially, and most of electric charge and the highest occupied molecular orbital (HOMO) are concentrated on sulfur; (2) the introduction of the oxygen atoms on sulfur in DPSO damages the aromatic system of DPS and also has a strong electron-withdrawing effect to inhabit polymerization.

Further experiments had been done to optimize the electrolytes for electrochemical polymerization of DNE and DPOB. Our results (some results were attached in Figure S2 of the Supporting Information) demonstrated that the optimum electrolytes are BFEE containing 10% concentrated SA (by volume) for DNE and BFEE for DPOB, respectively. It was interestingly found that the addition of SA into BFEE not only enhances the redox activity of as-formed PDNE but also synchronously improved the adherence of the films against the electrode and led to more uniform electrodeposition.

Potentiostatic electrolysis was employed to prepare the polymer films for characterization. To optimize the applied potentials for polymerization, a set of current transients during the electropolymerization of DNE and DPOB at different applied potentials in BFEE or BFEE-based mixed electrolytes were recorded, as shown in Figures S3 and S4. Considering the overall factors affecting the quality of the formed film, such as moderate polymerization rate, negligible overoxidation, regular morphology, and good adherence against the working electrode, the selected applied potentials are 0.9 V for DNE in BFEE + 10% SA, 1.0 V for DNE in BFEE, and 1.1 V for DPOB in BFEE.

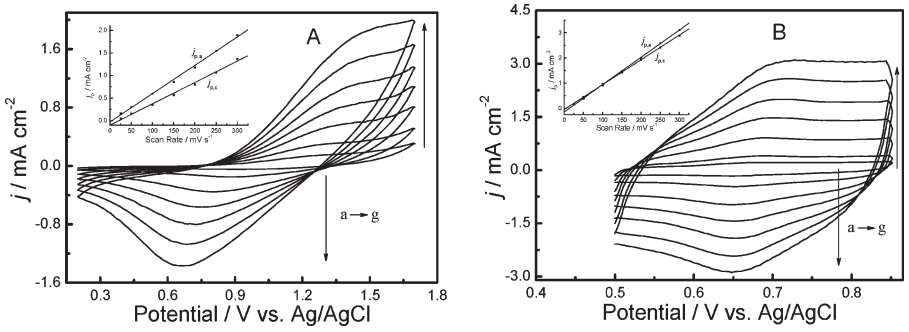

Figure 3. CVs of PDPOB films in monomer-free BFEE (A) and in concentrated SA (B) at potential scan rates of (a) 25, (b) 50, (c) 100, (d) 150, (e) 200, (f) 250, and (g) 300 mV s^{-1}. Inset: plots of redox peak current densities vs potential scan rates. j_p is the peak current density, and $j_{p,a}$ and $j_{p,c}$ denote the anodic and cathodic peak current densities, respectively.

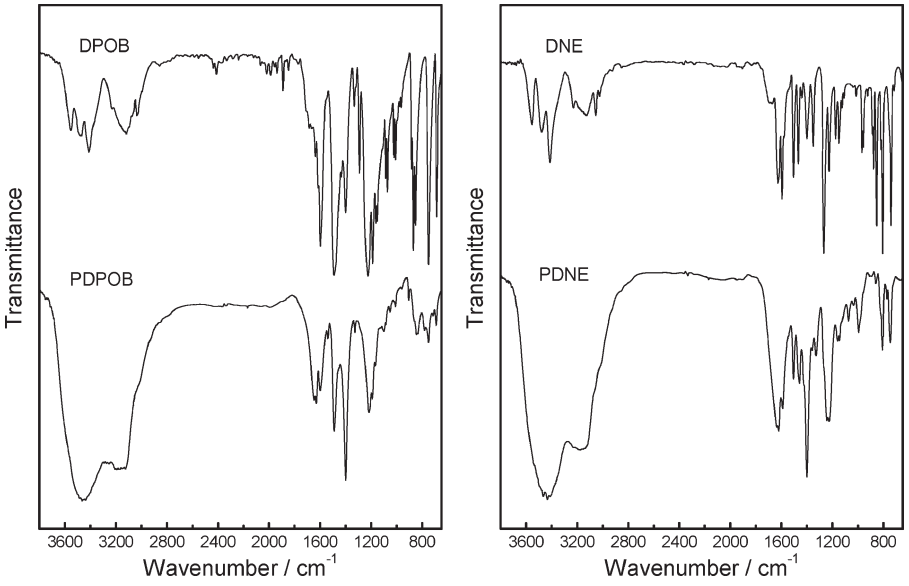

Figure 4. FT-IR spectra of DPOB, dedoped PDPOB, DNE, and dedoped PDNE.

3.2. Electrochemistry of PDNE and PDPOB Films. In order to get a deeper insight into the electrochemical and environmental stability of as-formed polymer films and their electroactivity, the electrochemical behavior of PDNE and PDPOB films was determined carefully by cyclic voltammetry in different monomer free electrolytes for comparison, as shown in Figure 2, Figure 3, and Figure S5, respectively. It can be clearly seen that steady-state CVs of these films represented broad anodic and cathodic peaks in all these electrolytes. The peak current densities were proportional to potential scanning rates (insets of Figure 2, Figure 3, and Figure S5), indicating that the redox process is nondiffusional and the electroactive polymer is well adhered to the working electrode surface. Furthermore, these films could be cycled repeatedly between the conducting (oxidized) and insulating (neutral) state without significant decomposition of the materials, indicating high redox stability of the polymer.

PDNE-coated electrodes prepared from both BFEE (Figure S5) and BFEE-SA were tested in monomer free electrolytes and in concentrated SA. By comparison, it is clear that the addition of SA into BFEE afforded better redox activity and stability of PDNE. The potentials needed to oxidize or reduce the polymer film prepared from the binary solvent system were from 0.62 to 0.26 V in monomer-free BFEE-SA (Figure 2A) and from 0.60 to 0.41 V in concentrated SA (Figure 2B). PDPOB films prepared from BFEE also exhibited good redox activity and stability in monomer-free BFEE (Figure 3A) and concentrated SA (Figure 3B). The polymer films could be oxidized and reduced from 1.52 to 0.72 V in BFEE and from 0.73 to 0.65 V in concentrated SA.

3.3. Structural Characterization. In order to elucidate the structure of the polymers and interpret the polymerization mechanism, FT-IR spectra of the monomers and doped polymer films were recorded, as shown in Figure 4. As can be seen from the figure, the absorption bands in the spectra of the doped polymers were obviously broadened in comparison with those of the monomers, similar to those of other conducting polymers reported previously.[10−18] This instance was mainly due to the resulting product composed of oligomers/polymers with wide chain dispersity. In more detail, the vibrational modes of the polymers with different polymerization degrees show different IR shifts. These peaks overlapped one another and produced broad bands with hyperstructures. Furthermore, the chemical defects on the polymer chains resulting from the overoxidation of the polymer also contributed to the band broadening of IR spectra.

The strong and narrow peaks at 751 and 688 cm^{-1} in the spectrum of DPOB were the characteristic absorption of the out-of-plane bending mode on monosubstituted benzene ring, while the 869 and 852 cm^{-1} bands ascribed to two adjacent carbon−hydrogen bonds (Figure 4).[18,29] After

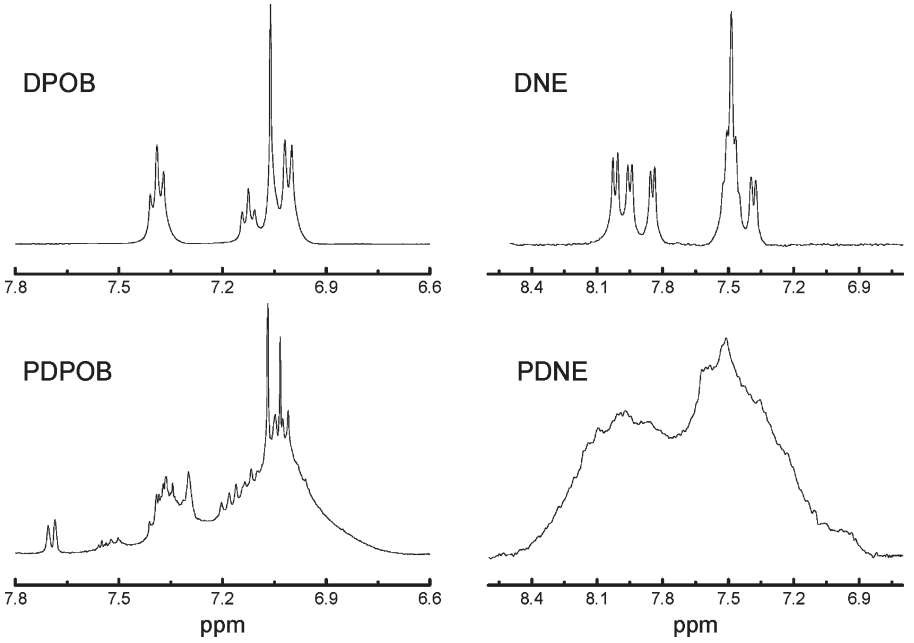

Figure 5. ^{1}H NMR spectra of DPOB, dedoped PDPOB, DNE, and dedoped PDNE. Solvent: d_6-DMSO.

Scheme 2. Possible Structures of Dedoped and Doped PDPOB and PDNE

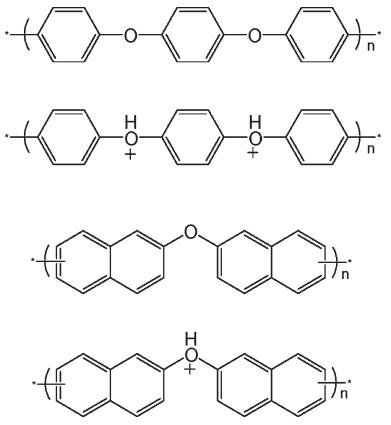

polymerization, the newly emerged bands at 845, 834, and 783 cm^{-1} implied that the polymerization occurred mainly through the coupling of *para*-positions on DPOB, same as that of DPE.[18,29] As to DNE, those bands centered at 878, 853, 807, and 717 cm^{-1} were assigned to 1,2,4-trisubstituted benzene ring.[29,30] The medium strong band at 742 cm^{-1} was closely related to the out-of-plane vibration of four adjacent carbon−hydrogen bonds on ortho-disubstituted benzene, which shifted to 747 cm^{-1} in the spectrum of PDNE (Figure 5).[29−31] In contrast, another band at 809 cm^{-1} in the spectrum of PDNE could be interpreted to be the absorption of 1,2,3,4-tetra-substituted benzene. Moreover, the absence of the absorption peaks at 878, 853, and 717 cm^{-1} manifested the occurrence of the polymerization, and the reaction sites may be α-positions of the naphthyl rings.

Interestingly, the strong and broad absorption emerged at 3500 cm^{-1} in the spectra of both PDPOB and PDNE compared with the spectra of the monomers, indicating the existence of OH in the polymer. This may be ascribed to the proton-doping properties of the polymers, and the proton dopants come from the deprotonization of the radical cations during the electrochemical polymerization. Together with our preliminary results, poly(aromatic ethers) probably own similar proton-doping nature to polyaniline, and the proposed structures of them are illustrated in Scheme 2.

To further investigate the polymer structure and the polymerization mechanism of DPOB and DNE, ^{1}H NMR spectra of the monomers and the soluble part of dedoped polymers were recorded in d_6-DMSO, as shown in Figure 5. From the figures, compared with the monomers, the polymers both showed very broad unresolved "hill", probably due to a complex mixture of oligomers with different chain lengths. The wide molar mass distribution of polymer or the complex structure of the polymers led to slightly different environment of the atoms. Because of the introduction of higher conjugation length onto the polymer main chain, the chemical shift of some C−H bonds moved to lower field.

For PDPOB, the existence of the proton chemical shift at 7.69 ppm (d, $^3J_{HH}$ = 7.8 Hz) indicated that DPOB mainly electropolymerized through the coupling at *para*-positions of the benzene ring. Although the spectrum of PDNE cannot provide distinct and lucid information about the structure of the polymer, it confirmed the occurrence of the electrochemical polymerization among the monomers.

Quantum chemical calculations can be applied effectively in the search for the structural study of newly obtained polymers. Optimized geometries of DPOB and DNE are shown in Scheme S2. DPOB exhibited more planar structure with a smaller dihedral angle (68.7°) than that of DNE (70.9°). Calculations for atomic electron density populations of DPOB (Scheme S3 and Table S1) showed similar negative electrons on each of its main atoms, while for DNE, the negative charge was mainly concentrated on α-positions of the naphthyl ring, e.g., C_1, C_4, C_5, C_8 and $C_{1'}$, $C_{4'}$, $C_{5'}$, $C_{8'}$, which implied that these atoms will donate electrons during the electrochemical polymerization. According to the frontier molecular orbital theory, the reaction between the active molecules mainly happens on the highest frontier molecular orbitals. The HOMO proportions of atoms C_1, C_3, C_4, C_6, $C_{4'}$, and $C_{4''}$ in DPOB were higher than those of other atoms (Scheme 3 and Table S2). It should be noted here that there

was considerable steric hindrance on C_3 and C_6 sites. As for DNE (Scheme 3 and Table S3), superior proportions in HOMO were observed at C_1, C_6, C_8 and $C_{1'}$, $C_{6'}$, $C_{8'}$ positions. On the basis of these results, it can be reasonably deduced that the polymerization sites of DPOB are preferentially $C_{4'}$ and $C_{4''}$ positions, while the polymerization of DNE might be complex.

By analogy with benzenes and anilines as coupling involves monomer radical cations during electrochemical polymerization, the most likely coupling sites are believed to be those with the largest electron spin density (ESD), where there will be the highest propensity for radical-coupling and bond formation. The calculated spin density distribution in the radical cations (Scheme 3 and Table S4) showed the highest unpaired ESD at C_1, C_4, $C_{4'}$, and $C_{4''}$ in DPOB while at C_1, C_6, C_8 and $C_{1'}$, $C_{6'}$, $C_{8'}$ positions in DNE. These calculations further confirmed the deduction mentioned above, and the polymerization of DNE would happen preferentially at C_1, C_6, C_8 and $C_{1'}$, $C_{6'}$, $C_{8'}$ positions.

3.4. Solubility, Molecular Weight Measurements, and UV−vis Spectra. As-formed PDPOB and PDNE films were both in the doped state, metallic dark green and dark brown in color, respectively. After dedoping with 25% ammonia, their color changed to bright brown and dark gray. Both doped and dedoped PDPOB and PDNE films were partly soluble in many common organic solvents, such as acetonitrile, DMSO, dichloromethane, tetrahydrofuran, chloroform, and even methanol, ethanol, acetone, diethyl ether, etc.

GPC measurements of the soluble part of the polymers in tetrahydrofuran demonstrated that the soluble part of PDPOB showed a number-average molar mass (M_n) of about 3200 and weight-average molar mass (M_w) of 4600 in tetrahydrofuran, while those of soluble PDNE were 2969 (M_n) and 4409 (M_w). The composition of soluble polymers in DMSO was also characterized by MALDI-TOF mass spectrometry, as shown in Figure S6. For PDNE, the obtained spectra were complex, but the m/z value varies in the range from about 400 to 2780, indicating that as-formed PDNE were mainly composed of relatively short-chain oligomers with 2−10 repetitive units, of which dimers, trimers, and tetramers contributed a large proportion. However, surprisingly, only three peaks characterized the MALDI-TOF mass spectrum of PDPOB at m/z = 904, 1831, and 4534, corresponding to 3, 7, and 17 repetitive DPOB units, respectively. This is mainly due to the relatively poor solubility of free-standing PDPOB films.

UV−vis spectra of the monomers and the resulting polymers in DMSO were examined, as shown in Figure 6A,B. DPOB showed two characteristic absorption peaks at 271 and 278 nm (Figure 6A-a) while DNE (Figure 6B-c) at 265 and 315 nm, 329 nm (a single electron $\pi-\pi^*$ transition). It can be clearly seen that, due to the increase in the conjugated chain length, the overall absorption of the polymers tailed off to more than 490 nm for PDPOB (Figure 6A-b) and about 680 nm for PDNE (Figure 6B-d) in comparison with that of the monomer (312 nm for DPOB and 342 nm for DNE), respectively. These spectral results confirmed the occurrence of electrochemical polymerization among the monomers and the formation of a conjugated polymer with broad molar mass distribution. Moreover, UV−vis spectra of doped and

Scheme 3. Main Composition and Proportion of the Frontier Orbitals and Atomic Electron Spin Densities (ESD) in DPOB and DNE (%)[a]

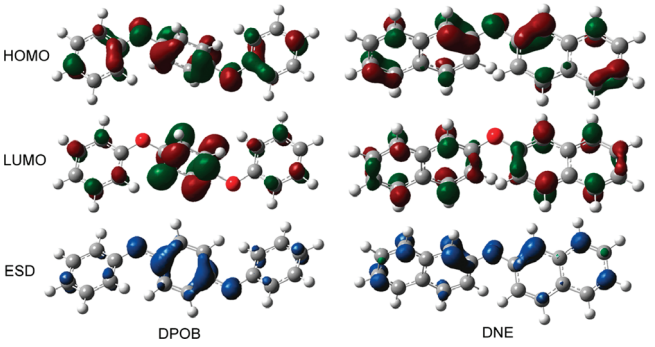

[a] HOMO and LUMO are defined as the highest occupied molecular orbital and the lowest unoccupied molecular orbital.

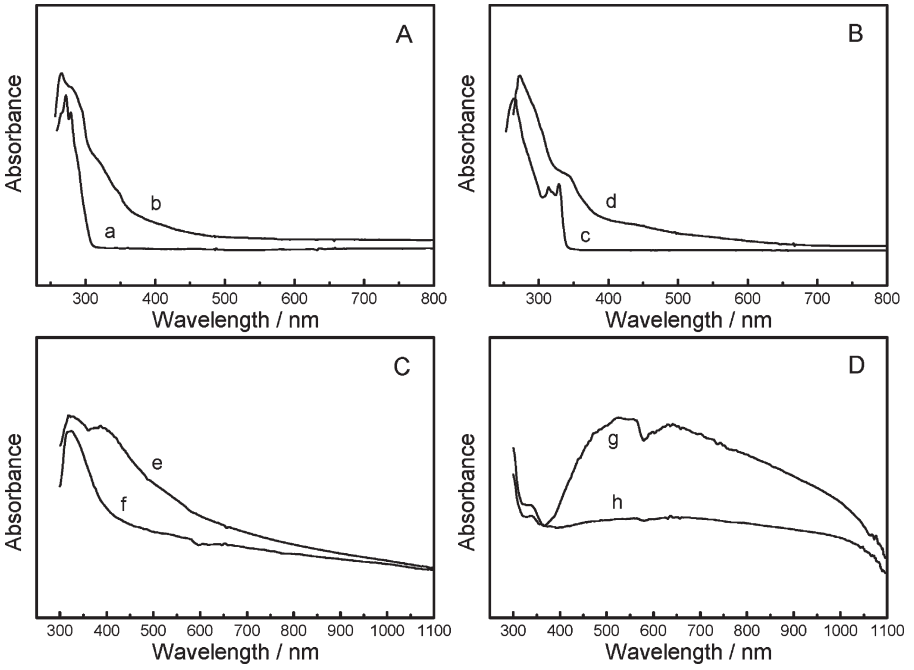

Figure 6. UV−vis spectra of the monomers and dedoped polymers in DMSO (A, B) and in solid state (C, D) as indicated: (a) DPOB; (b) dedoped PDPOB; (c) DNE; (d) dedoped PDNE; (e) doped PDPOB; (f) dedoped PDPOB; (g) doped PDNE; (h) dedoped PDNE.

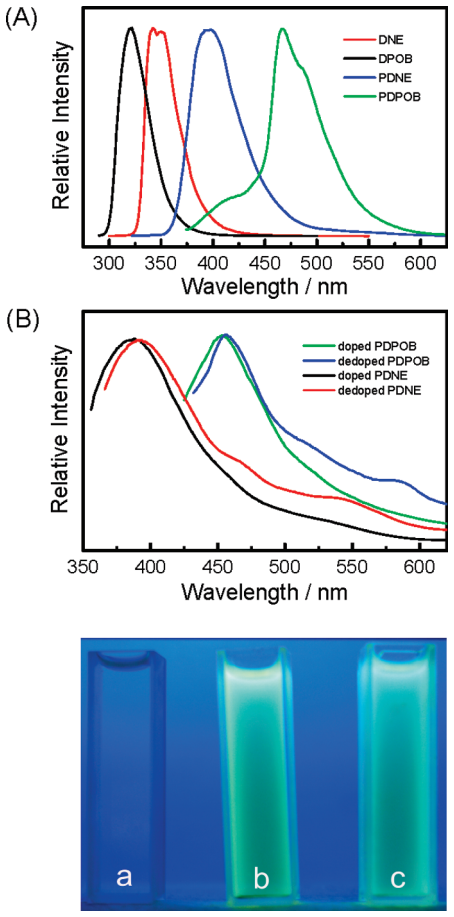

Figure 7. Fluorescence spectra of the monomers and the polymers in DMSO (A) and in solid state (B) as indicated and photoluminescence of PDPOB in THF under 365 nm UV irradiation (a: DPOB; b: doped PDPOB; c: dedoped PDPOB).

dedoped PDPOB and PDNE were quite similar, mainly depending on the automatic dedoping process of the polymer, concerning dopant removal.

UV−vis spectra of PDPOB and PDNE deposited on ITO transparent electrode are also depicted in Figure 6C,D. Both doped and dedoped PDPOB (Figure 6C) showed the same absorption at 322 nm, and the similar results could be found between doped and dedoped PDNE (Figure 6D) at 332 nm. However, the doped polymers showed other broad absorptions centered at 390 nm (PDPOB) and 532 nm, 640 nm (PDNE), which could be attributable to the characteristics of the existence of conductive species, such as polarons or bipolarons.

3.5. Fluorescence Spectra. The fluorescence emission spectra of the monomers and the dedoped polymers were determined both in DMSO and in the solid state, as shown in Figure 7. The emission spectrum of DPOB (Figure 7A) emerged at 320 nm in DMSO when excited at 281 nm, whereas a maximum emission peak at 467 nm characterized the spectrum of dedoped PDPOB (excited at 347 nm). For DNE, it exhibited a strong emission peak at 343 nm under excitation at 290 nm, and it is observed that the emission of its polymer centered at 395 nm at 296 nm excitation. Large red shifts between the monomer and the polymer (about 147 and 52 nm) can be clearly seen from the figure, which is mainly attributable to the elongation of the polymer's delocalized π-electron chain sequence. It should be noted here that PDNE showed remarkable blue shift compared with the emission of electropolymerized polynaphthalene (417 nm),[30,31] probably because the substitution of oxygen decreases the effective conjugated chain length of as-formed polymer based on the following two reasons: (1) increasing steric hindrance; (2) stabilizing the radical cations due to its electron-donating nature. Because of the introduction of phenoxy group substitution, a bathochromic shift of about 16 nm arose in the emission spectra of PDPOB compared with that of PDPE (451 nm). In solid state, slight hypsochromic shifts of 5−10 nm were found in Figure 7B, which may be attributed to the interaction of adjacent polymer chains in polymer matrix. Additionally, there was no much difference from the emission spectra between the doped polymers and the dedoped ones.

In DMSO, the fluorescence quantum yield ($\phi_{overall}$) of PDPOB was calculated to be 0.40 according to eq 2, higher than that of PDPE (0.30),[18] whereas that of soluble PDNE films was 0.18. Meanwhile, it is also very interesting to find that soluble PDPOB dissolved in common organic solvents, such as methanol, ethanol, acetone, acetonitrile, diethyl ether, DMSO, etc., can all emit strong blue-green photoluminescence when exposed to 365 nm UV light, as shown in Figure 7, whereas the monomers and PDNE showed no emission. It should be noted here that doped PDPOB showed slight weaker emission light than the dedoped polymer, mainly because the dopants in doped polymer led to fluorescence quenching among the polymer matrix.

Combined with our preliminary results,[18] poly(aromatic ethers) showed good blue light-emitting properties and it is quite expected that they may be used as fluorescence materials and electroluminescent materials. Apparently, the fluorescence properties (including the emissive wavelength and

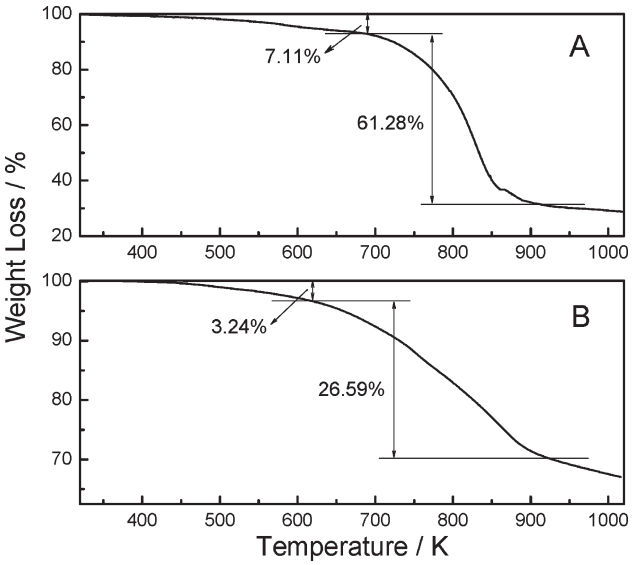

Figure 8. TGA curves of dedoped PDPOB (A) and PDNE (B) films under a nitrogen atmosphere.

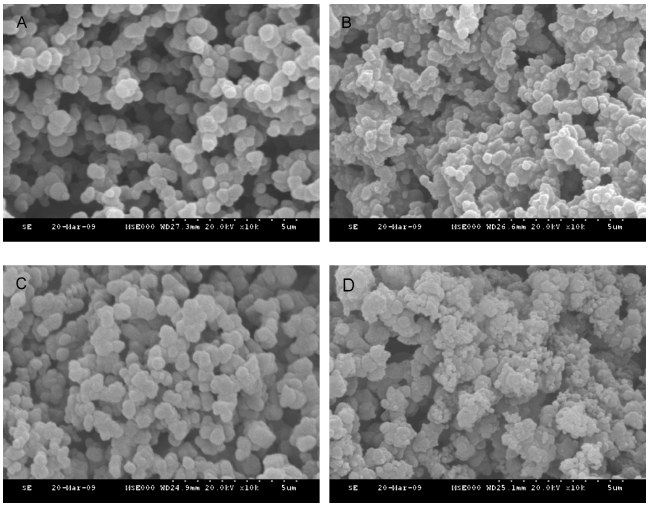

Figure 9. SEM photographs of PDPOB and PDNE films deposited electrochemically on ITO electrode for 400 s: (A, B) doped and dedoped PDPOB; (C, D) doped and dedoped PDNE. Magnification: 10000×.

intensity) can be tuned by functionalization at different positions with different groups.

3.6. Thermal Analysis. Thermal degradation behavior of conducting polymers is very important for their potential applications. For most conducting polymers, the skeletal decomposition temperatures are usually low, generally reported to be lower than 600 K, which hinders their practical uses in various fields. To investigate the thermal stability of the newly obtained polymers, thermogravimetric analytical experiments were performed under a nitrogen stream, as shown in Figure 8. For comparison, the thermogravimetric curves of the monomers were also examined (Figure S7). From the figure, it can be clearly observed that there were both three-step weight losses for PDNE (Figure 8A) and PDPOB (Figure 8B). The polymer initially underwent a small weight decrease (about 7.11% for PDNE and 3.24% for PDPOB) at relatively low temperature (from 300 to 694 K for PDNE and from 300 to 623 K for PDPOB), which may be attributed to water evaporation and other moisture or a few oligomers trapped in the polymer according to many authors. With the gradual increasing of the temperature, a prominent weight loss step (about 61.28% for PDNE, 26.59% for PDPOB) was clearly found at 694 K < T < 925 K and 623 K < T < 922 K, respectively, which were essentially due to the oxidizing decomposition of the skeletal PDNE and PDPOB backbone chain structures. The corresponding maximal decomposition of the polymers appeared at 832 and 844 K, respectively. The following degradation after 925 or 922 K was probably caused by the overflow of the oligomers decomposed from the polymer main chains, as mentioned previously. In addition, even when the temperature reached 1000 K, the residual weight of the polymer films were 31.61% and 70.17%, respectively. In contrast, the monomers bore an analogy with each other, both decomposing initially at 438 K and over at 556 K. Moreover, PDNE and PDPOB have higher thermal stability than most of the conducting polymers reported previously, which can be mainly ascribed to the high thermal stability of benzene ring incorporation into the main chain of as-formed polymer films. Therefore, from all these results, the conclusion can be easily drawn that the as-prepared PDNE and PDPOB films display high decomposition temperatures, indicating that they can be applied in

a wide temperature scale, which is of special significance for some potential applications.

3.7. Conductivity and Morphology. According to eq 1, the electrical conductivity of the pressed pellets of doped PDNE obtained from BFEE + 10% SA was measured to be 7.1×10^{-3} S cm^{-1}, while that of PDPOB was 1.6×10^{-1} S cm^{-1} as free-standing films, both lower than that of PDPE films (4.4×10^{-1} S cm^{-1}).[18] This phenomenon can be correlated to a decrease of the average length of the conjugated π-system in PDNE and PDPOB. This limited conjugation can be explained by considering the changes in the reactivity of the monomers resulting from the delocalization of the π-electrons over the entire molecules. Namely, the overall reactivity of the monomers decreases or, in other words, the stability of the corresponding radical cations increases, which causes a decrease or even in some cases a complete loss of polymerizability. On the other hand and as already known, during the initial stage of polymerization, the conjugated structures of the formed oligomers probably result in decreases in the relative reactivity of the proposed positions, which has deleterious consequences for the stereoselectivity of polymerization.

Additionally, the electrical conductivity of dedoped PDPOB in pressed pellets was measured to be 10^{-9} S cm^{-1}. After immersed into hydrochloric acid (12 mol L^{-1}) for 6 h and then dried under vacuum, it was observed that the conductivity of the same sample (10^{-6} S cm^{-1}) was increased several orders of magnitude. This difference further proved proton-doping properties of as-formed poly(aromatic ethers).

Scanning electron microscopy (SEM) photographs (Figure 9) showed that both PDNE and PDPOB films displayed sphere-type growth processes whereby a number of clusters were observed from Figure 9A,C, similar to surface morphology of PDPE. This growth mode is a feature of stronger interactions between deposited molecules than between the film and substrate. Another possible reason is that the amount of precursor is sufficient to form a layer of thin film and then some microspheres (with diameters in the range from 200 nm to 1 μm). Further, this morphology facilitates the movement of doping anions in and out of the polymer films during doping and dedoping processes, in well accordance with the good redox activity of PDNE and PDPOB films in the monomer-free electrolytes. Nevertheless, the surface morphologies of the dedoped polymer films (Figure 9B,D) transformed evidently, and the nanospheres were partly destroyed. These differences between the doped and dedoped polymer films of both PDNE and PDPOB were mainly due to the migration of counteranions out of the polymer films and their gradual solubility from the electrode to the solution during the dedoping processes, which broke the relatively smooth surfaces of doped polymer films.

4. Conclusions

To summarize, the electrochemical performances of a series of aromatic ethers have been systematically investigated, and it is found that direct anodic oxidation of DPOB and DNE can lead to successful deposition of their polymers while DPS and DPSO are incapable of electropolymerization, probably due to the significant influences of the sulfur/sulfonyl group substitution on the electronic structure of the molecules. Full characterization of the resulting polymers showed that poly(aromatic ethers) exhibited favorable electrical conductivity, good redox activity, high fluorescence, excellent thermal stability, and uniform morphology. More importantly, poly(aromatic ethers) probably showed proton-doping properties similar to polyanilines. This opens up the prospect of exploiting the attractive properties of poly(aromatic ethers) in applications of thin-film materials. In particular, different precursors on each side of the ether and judicious substitution on nonpolymerizable sites, such as *ortho*-position of the ether linkage, should enable the tuning of film characteristics for specific enhancement of thin-film properties, including film composition, conductivity, homogeneity, redox potentials, and luminescence properties. It is also very interesting to find that conducting poly(aromatic ethers) probably show proton-doping nature, bearing analogy with polyaniline. Therefore, these materials open up a new, unexplored, and potentially vast area of research on poly(aromatic ethers) and hold promise for the design of a new generation of optoelectronic materials.

Acknowledgment. NSFC (50663001, 50963002, and 20874112) and Jiangxi Jinggang Star Project are acknowledged for their financial ssupport.

Supporting Information Available: Cyclic voltammograms and chronoamperograms of DNE/DPOB in different electrolytes; cyclic voltammograms of PDNE films from BFEE in different media as indicated; computational results; MALDI-TOF mass spectra; thermogravimetric curves of DNE and DPOB. This material is available free of charge via the Internet at http://pubs.acs.org.

References and Notes

(1) Shirakawa, H.; Louis, E. J.; MacDiarmid, A. G.; Chiang, C. K.; Heeger, A. J. *J. Chem. Soc., Chem. Commun.* **1977**, 578–580.
(2) Skotheim, T. A.; Reynolds, J. R. *Handbook of Conducting polymers*, 3rd ed., CRC: Boca Raton, FL, 2007.
(3) Boudreault, P. L. T.; Wakim, S.; Blouin, N.; Simard, M.; Tessier, C.; Tao, Y.; Leclerc, M. *J. Am. Chem. Soc.* **2007**, *129*, 9125–9136.
(4) Roncali, J. *Chem. Rev.* **1992**, *92*, 711–738.
(5) Neher, D. *Macromol. Rapid Commun.* **2001**, *22*, 1366–1385.
(6) Leclerc, M. *J. Polym. Sci., Polym. Chem.* **2001**, *39*, 2867–2873.
(7) Scherf, U.; List, E. J. W. *Adv. Mater.* **2002**, *14*, 477–487.
(8) Sonmez, G.; Shen, C. K. F.; Rubin, Y.; Wudl, F. *Angew. Chem., Int. Ed.* **2004**, *43*, 1498–1502.
(9) Lévesque, I.; Bertrand, P.; Blouin, N.; Leclerc, M.; Zecchin, S.; Zotti, G.; Ratcliffe, C. I.; Klug, D. D.; Gao, X.; Gao, F. M.; Tse, J. S. *Chem. Mater.* **2007**, *19*, 2128–2138.
(10) Zhou, W. Q.; Peng, H. P.; Xu, J. K.; Xia, H. Y.; Pu, S. Z. *Polym. Int.* **2008**, *57*, 92–98.
(11) Nie, G. M.; Han, X. J.; Zhang, S. S.; Wei, Q. L. *J. Polym. Sci., Polym. Chem.* **2007**, *45*, 3929–3940.
(12) Fan, B.; Qu, L. T.; Gao, G. Q. *J. Electroanal. Chem.* **2005**, *575*, 287–292.
(13) Xu, J. K.; Hou, J.; Zhang, S. S.; Xiao, Q.; Zhang, R.; Pu, S. Z.; Wei, Q. L. *J. Phys. Chem. B* **2006**, *110*, 2643–2648.
(14) Lu, B. Y.; Xu, J. K.; Fan, C. L.; Jiang, F. X.; Miao, H. M. *Electrochim. Acta* **2008**, *54*, 334–340.
(15) Qu, L. T.; Shi, G. Q. *Chem. Commun.* **2004**, 2800–2801.
(16) Lu, G. W.; Shi, G. Q. *J. Electroanal. Chem.* **2006**, *586*, 154–160.
(17) Lu, B. Y.; Xu, J. K.; Fan, C. L.; Miao, H. M.; Shen, L. *J. Phys. Chem. B* **2009**, *113*, 37–48.
(18) Xu, J. K.; Wan, L.; Li, Y. Z.; Liu, H. T.; Pu, S. Z.; Shen, L. *J. Polym. Sci., Polym. Chem.* **2007**, *45*, 5932–5941.
(19) Lakowicz, J. R. *Principles of Fluorescence Spectroscopy*, 2nd ed.; Kluwer Academic/Plenum: New York, 1999.
(20) Frisch, M. J.; Trucks, G. W.; Schlegel, H. B.; Scuseria, G. E.; Robb, M. A.; Cheeseman, J. R.; Montgomery, J. A.; Jr., Vreven, T.; Kudin, K. N.; Burant, J. C.; Millam, J. M.; Iyengar, S. S.; Tomasi, J.; Barone, V.; Mennucci, B.; Cossi, M.; Scalmani, G.; Rega, N.; Petersson, G. A.; Nakatsuji, H.; Hada, M.; Ehara, M.; Toyota, K.; Fukuda, R.; Hasegawa, J.; Ishida, M.; Nakajima, T.; Honda, Y.; Kitao, O.; Nakai, H.; Klene, M.; Li, X.; Knox, J. E.; Hratchian, H. P.; Cross, J. B.; Adamo, C.; Jaramillo, J.; Gomperts, R.; Stratmann, R. E.; Yazyev, O.; Austin, A. J.; Cammi, R.; Pomelli, C.; Ochterski, J. W.; Ayala, P. Y.; Morokuma, K.; Voth, G. A.;

Salvador, P.; Dannenberg, J. J.; Zakrzewski, V. G.; Dapprich, S.; Daniels, A. D.; Strain, M. C.; Farkas, O.; Malick, D. K.; Rabuck, A. D.; Raghavachari, K.; Foresman, J. B.; Ortiz, J. V.; Cui, Q.; Baboul, A. G.; Clifford, S.; Cioslowski, J.; Stefanov, B. B.; Liu, G.; Liashenko, A.; Piskorz, P.; Komaromi, I.; Martin, R. L.; Fox, D. J.; Keith, T.; Al-Laham, M. A.; Peng, C. Y.; Nanayakkara, A.; Challacombe, M.; Gill, P. M. W.; Johnson, B.; Chen, W.; Wong, M. W.; Gonzalez, C.; Pople, J. A. *Gaussian 03, Revision C.02*; Gaussian, Inc.: Wallingford, CT, 2004.

(21) Parr, R. G.; Yang, W. *Density-Functional Theory of Atoms and Molecules*; Oxford University Press: New York, 1989.

(22) Koch, W.; Holthausen, M. C. *A Chemist's Guide to Density Functional Theory*; Wiley-VCH: New York, 2000.

(23) Lee, C.; Yang, W.; Parr, R. G. *Phys. Rev. B* **1988**, *37*, 785–789.

(24) Becke, A. D. *J. Chem. Phys.* **1993**, *98*, 5648–5652.

(25) Chen, W.; Xue, G. *Prog. Polym. Sci.* **2005**, *30*, 783–811.

(26) Shi, G. Q.; Jin, S.; Xue, G.; Li, C. *Science* **1995**, *276*, 994–996.

(27) Shi, G. Q.; Li, C.; Liang, Y. Q. *Adv. Mater.* **1999**, *11*, 1145–1146.

(28) Jin, S.; Xue, G. *Macromolecules* **1997**, *30*, 5753–5757.

(29) Rong, G. B.; Zhu, S. Z. *Structure Determination of Organic Compounds—Tables of Spectral Data*; East China University of Science and Technology Press: Shanghai (in Chinese), 2002.

(30) Huang, Z. M.; Shi, G. Q.; Qu, L. T.; Hong, X. Y. *J. Electroanal. Chem.* **2003**, *544*, 41–46.

(31) Huang, Z. M.; Qu, L. T.; Shi, G. Q.; Chen, F. E.; Hong, X. Y. *J. Electroanal. Chem.* **2003**, *556*, 159–165.